



Lung surfactant negatively affects the photodynamic inactivation of bacteria—in vitro and molecular dynamic simulation analyses

Giulia Kassab^a , Johan Sebastian Diaz Tovar^a, Lucas Miguel Pereira Souza^b, Rayla Kelly Magalhães Costa^b, Rudielson Santos Silva^b, André Silva Pimentel^b, Cristina Kurachi^a , and Vanderlei Salvador Bagnato^{a,c,1}

Contributed by Vanderlei Salvador Bagnato; received December 31, 2021; accepted April 5, 2022; reviewed by Colin Hopper and Véronique Rosilio

In the context of the rapid increase of antibiotic-resistant infections, in particular of pneumonia, antimicrobial photodynamic therapy (aPDT), the microbiological application of photodynamic therapy (PDT), comes in as a promising treatment alternative since the induced damage and resultant death are not dependent on a specific biomolecule or cellular pathway. The applicability of aPDT using the photosensitizer indocyanine green with infrared light has been successfully demonstrated for different bacterial agents in vitro, and the combination of pulmonary delivery using nebulization and external light activation has been shown to be feasible. However, there has been little progress in obtaining sufficient in vivo efficacy results. This study reports the lung surfactant as a significant suppressor of aPDT in the lungs. In vitro, the clinical surfactant Survanta® reduced the aPDT effect of indocyanine green, Photodithazine®, bacteriochlorin-trizma, and protoporphyrin IX against *Streptococcus pneumoniae*. The absorbance and fluorescence spectra, as well as the photobleaching profile, suggested that the decrease in efficacy is not a result of singlet oxygen quenching, while a molecular dynamics simulation showed an affinity for the polar head groups of the surfactant phospholipids that likely impacts uptake of the photosensitizers by the bacteria. Methylene blue is the exception, likely because its high water solubility confers a higher mobility when interacting with the surfactant layer. We propose that the interaction between lung surfactant and photosensitizer must be taken into account when developing pulmonary aPDT protocols.

lung surfactant | Survanta | photosensitizers | photodynamic therapy | antimicrobial

Lower respiratory tract infections are the leading infectious cause of death worldwide (1). The emergence of new respiratory pandemics and the antibiotic-based therapy crisis drive a desperate need for new treatment approaches that are effective against multiple pathogens and unlikely to select for resistance (2, 3). Antimicrobial photodynamic therapy (aPDT) comes in as a promising alternative for the treatment of respiratory infections. It is based on the combination of a photosensitizer (PS), light at a specific wavelength, and molecular oxygen to generate reactive oxygen species (ROS) that induce oxidative damage and lead to cell death (4). Since it is not targeting one specific biomolecule or cellular pathway, it can be used for the treatment of multiple pathogens, including bacteria, fungi, virus, and protozoa (5). Another benefit of aPDT is its double selectivity achieved from the PS accumulation in the infectious agents over the hosts cells and the restricted exposure to light on the affected area, reducing undesired systemic effects (6).

The combination of the PS indocyanine green (ICG) and external activation with infrared light was initially proposed for the treatment of pulmonary infections by our research group in 2014 (as described in *SI Appendix, Fig. S1*) (7, 8). In 2018, Leite et al. (9) showed that it was possible to eliminate *Streptococcus pneumoniae* using doses of ICG and light that were unharmed to macrophages. Moreover, there was evidence that the aPDT could potentialize the antimicrobial activity of such macrophages during the infection (9). In 2019, Kassab et al. (10) proposed nebulization as a new delivery method, demonstrated its compatibility with ICG, and validated the delivery in an animal model. Meanwhile, Wong et al. (11) found that methicillin-resistant strains of *Staphylococcus aureus* were more susceptible to ICG–aPDT than methicillin-susceptible strains. They also reported a reversion of the resistant phenotype in one of the strains after the aPDT treatment (11). In 2020, pulmonary ICG–aPDT in mice was shown to be safe for the host and able to activate the PS using extracorporeal irradiation in this model (12). Finally, in 2021, Tovar et al. (13) demonstrated the activation of ICG and its photodynamic inactivation (PDI) effect in *S. pneumoniae* when illuminated through

Significance

Understanding the interaction between drugs and the microenvironment of their target is fundamental for the development of new treatments. In this study, we report how the lung surfactant, a combination of phospholipids and proteins that covers the air–lung interface, may interact with and hinder the efficacy of different antimicrobial photosensitizers. Antimicrobial photodynamic therapy is a promising alternative to antibiotics since it does not depend on a specific biomolecule or cellular pathway. However, the clinical surfactant Survanta® reduces the in vitro antimicrobial effect of indocyanine green, Photodithazine®, bacteriochlorin-trizma, and protoporphyrin IX against *Streptococcus pneumoniae*. Methylene blue is the exception, likely because of its higher mobility when interacting with the surfactant layer as seen using molecular dynamics simulations.

Author contributions: G.K., A.S.P., C.K., and V.S.B. designed research; G.K., J.S.D.T., L.M.P.S., R.K.M.C., and R.S.S. performed research; G.K., J.S.D.T., L.M.P.S., R.K.M.C., R.S.S., A.S.P., C.K., and V.S.B. analyzed data; and G.K., J.S.D.T., L.M.P.S., R.K.M.C., R.S.S., A.S.P., C.K., and V.S.B. wrote the paper.

Reviewers: C.H., University College London; and V.R., Université Paris-Saclay.

The authors declare no competing interest.

Copyright © 2022 the Author(s). Published by PNAS. This article is distributed under [Creative Commons Attribution-NonCommercial-NoDerivatives License 4.0 \(CC BY-NC-ND\)](https://creativecommons.org/licenses/by-nc-nd/4.0/).

¹To whom correspondence may be addressed. Email: vander@ifsc.usp.br.

This article contains supporting information online at <http://www.pnas.org/lookup/suppl/doi:10.1073/pnas.2123564119/-DCSupplemental>.

Published June 13, 2022.

the thoracic cage in an ex vivo pig carcass, proposing a model for the light distribution in this scenario and suggesting that treatment times would be compatible with a clinical context. Pulmonary delivery using nebulization has also been proposed for other PSs, such as methylene blue (MB) and curcumin (14–16).

However, there has been little progress in terms of obtaining in vivo efficacy results in the photodynamic treatment of bacterial pneumonia. After many years invested in developing pneumonia models and improving aPDT parameters, it became clear that there was more to it than simply combining PS, light, and oxygen. Eventually, we hypothesized that the interaction between the PSs and the lung surfactant could be inhibiting the expected phototoxicity. The lung surfactant is a mixture of phospholipids and proteins that is expressed by the lung epithelium and presents two main purposes: enabling the gas exchange by decreasing the surface tension of the air–water interface and protecting the organism from contaminants in the air (17, 18). The decreased efficacy of antibiotics and other drugs in the presence of lung surfactant has been thoroughly reported in the literature (19–25). To investigate this possibility, five PSs with potential for aPDT applications in the lungs had their efficacy in killing the pneumonia-causing *S. pneumoniae* tested in the presence and absence of a medical-grade lung surfactant. Then, optical measurements and a molecular dynamics simulation were used to further explain the observed results and potential mechanisms. Understanding the interaction between PSs and the lung surfactant is a necessary step toward overcoming the challenges of using aPDT to treat pneumonia.

1. Methodology

1.1. Lung Surfactant, PSs, and Light Sources. Five PSs were chosen to provide a wide range of chemical and photochemical characteristics (Table 1). ICG (Ophthalmos) was solubilized in water for injection on the same day of each experiment. MB (Sigma-Aldrich) was prepared in phosphate-buffered saline (PBS) and stored at 4 °C. Photodithazine (PDZ; Fotoditazin) was diluted from the commercialized solution as needed and kept according to the manufacturer's instructions. Protoporphyrin IX (PpIX; Sigma-Aldrich) and bacteriochlorin-trizma (BC-t; provided by the Microbiology and Parasitology Laboratory and the Bio-Organic Chemistry Laboratory of the Federal University of São Carlos, Brazil) were diluted in dimethyl sulfoxide (DMSO) on the same day of each experiment. From the stock solutions, each PS was further diluted in PBS to the appropriate concentration before each experiment. The lung surfactant (Survanta®; AbbVie) was diluted in experiment solutions to achieve a final concentration of 5%, which was sufficient to observe inhibition effects in a similar study (22).

The light exposure was performed using custom-made devices developed by the technical support laboratory from the Institute of Physics of São Carlos of the University of São Paulo (Brazil). For ICG, laser devices were used, with peak emission at 808 nm (80 mW/cm² for the PDI experiment and 60 mW/cm² for the photobleaching assay). For all other PSs, the light sources were light-emitting diodes (LEDs), with peak emission at 780 nm for BC-t (30 mW/cm² for the PDI,

60 mW/cm² for the photobleaching assay) and 660 nm for MB, PDZ, and PpIX (50 mW/cm² for both experiments).

1.2. Bacterial Inactivation Assay. The gram-positive *S. pneumoniae* strain ATCC 49619 (American Type Cell Culture) was thawed from frozen stocks and grown in brain–heart infusion broth for 4 to 5 h (37 °C, 5% CO₂) until log phase. It was then centrifuged and resuspended in PBS, and the concentration was adjusted to 5.5 × 10⁶ colony-forming units (CFU) per mL. The bacterial suspension was distributed into 96- or 24-well plates, and either Survanta® or more PBS was added to the wells. The plates were placed in a shaker (150 rpm, 37 °C) for 30 min so that any surface adsorption phenomena or interaction between lung surfactant and bacteria would take place and stabilize before inserting the PS. Then, the PSs were added, and the plates were incubated in the dark (37 °C, no agitation) for 20 min. The final concentrations for each component during the aPDT treatment were 5.0 × 10⁶ CFU/mL of *S. pneumoniae*; 5% Survanta® (when present); and 10 μM ICG, 1 μM PpIX, 1 μM MB, 1 μM BC-t, or 100 nM PDZ. Samples were taken prior to the illumination and again after fluences of 10 and 20 J/cm². The samples were diluted, seeded onto blood agar, and incubated at 37 °C. After 18 to 24 h, the colonies were counted. Experiments were performed in triplicate on three separate occasions, totaling *n* = 9.

The data were processed using GraphPad Prism 8. The colony count units were transformed into log₁₀ so that a two-way repeated measure ANOVA could be used for statistical comparison. A post hoc Sidak's multiple comparisons test was used to compare the effect of the presence of Survanta® in each of the light doses. Results were considered to be significantly different with *P* < 0.05.

1.3. Optical Properties Measurements. The absorbance and fluorescence spectra were collected for the five PSs using a Cary 50-Varian Bio ultraviolet and visible (UV-Vis) spectrophotometer and a Cary Eclipse Fluorescence Spectrophotometer, respectively. Four-sided clear plastic cuvettes of 1-cm path length were prepared with either 950 μL PBS or 900 μL + 50 μL Survanta® and were left under agitation (150 rpm, 37 °C) for 30 min. Then, 50 μL of concentrated PS solutions (prepared as described previously) were added to the cuvettes, achieving a final concentration of 10 μM for each PS and 5% Survanta® when present. Absorbance was recorded at room temperature in the 300- to 900-nm range. The fluorescence spectra were collected for every PS at a specific wavelength according to Table 2. For the photobleaching measurements, a total fluence of 20 J/cm² was fractionated in 5-J/cm² increments, and then, the absorbance spectra were recorded. The absorbance at the wavelength of highest intensity was recorded and compared. All optical properties measurements were performed in triplicate from independent PS solutions. Data were initially processed using Origin 2018, in which a smoothing processing was applied to the spectra in order to remove the noise. The Savitzky–Golay method was used since it preserves the original shapes of the signal peaks (points of window: 50, polynomial order: 2, no boundary condition). Then, the data were plotted using GraphPad Prism 8. Absorbance and fluorescence spectra are plotted as the mean for each triplicate. The photobleaching data were compared using a two-way ANOVA with a post hoc Sidak's test to compare the effect of Survanta®.

1.4. Model Parameters Used for Molecular Simulation. Two symmetrical phospholipid monolayers were constructed using the program Packmol (1). A water box containing roughly 7,355 single-point charge water molecules was

Table 1. PSs used in this study and their key characteristics

| PS | Class | Molar mass (g/mol) | Absorption peak (nm) | ϵ (M ⁻¹ cm ⁻¹) | $\phi^1_{O_2}$ | Net charge* | LogP [†] |
|------|-----------------|--------------------|-------------------------|--|---------------------|-------------|-------------------|
| ICG | Cyanine | 775.0 | 780 | 205,000 (26) | Not detectable (27) | – | 4.17; 6.05 |
| MB | Phenothiazine | 319.9 | 670 | 71,089 | 0.49 (28) | + | 3.61; 2.61 |
| PpIX | Porphyrin | 562.7 | 365, 532, 557, 589, 641 | 47,433 (29) | 0.56 (28) | 2– | 5.9 |
| PDZ | Chlorin | 596.7 | 660 | 38,200 (30, 31) | ‡ | 3– | 4.6 |
| BC-t | Bacteriochlorin | 711.8 | 755 (32) | ‡ | ‡ | + | 4.4; 6.78 |

ϵ , molecular absorption coefficient; $\phi^1_{O_2}$, quantum yield of singlet oxygen formation.

*Net charge of the main microspecies at pH 7 (ChemAxom).

†Using the atom-additive method XLogP3-AA, in the program ALogPS (ChemAxom).

‡Not reported in the literature.

Table 2. Optical parameters for the fluorescence spectra measurements

| PS | $\lambda_{excitation}$ (nm) | $\lambda_{detection}$ (nm) |
|------|-----------------------------|----------------------------|
| ICG | 780 | 800–900 |
| MB | 660 | 680–800 |
| PDZ | 660 | 680–800 |
| BC-t | 780 | 800–900 |
| PpIX | 405 | 425–750 |

built between the monolayers, in contact with the phospholipid polar heads. The water box had the approximate dimensions of $6.3 \times 6.3 \times 6.0 \text{ nm}^3$, allowing enough displacement between the two monolayers that they did not interact with each other. Each PS was placed at the center of the water box. For simplification purposes, only the active chlorin e_6 portion of PDZ was used in the simulation, and the *N*-methyl glucosamine counterion was omitted. The entire system had the dimensions of $6.3 \times 6.3 \times 40 \text{ nm}^3$, which allowed for around 15 nm of vacuum above the upper monolayer and under the lower monolayer. The system was built as two symmetrical monolayers instead of one monolayer because the periodic boundary conditions would not allow the simulation of one monolayer, a water subphase, and the vacuum phase. The phospholipid monolayer consisted of dipalmitoyl phosphatidylcholine (DPPC), 1-palmitoyl-2-oleoyl phosphatidylcholine (POPC), dipalmitoyl phosphatidylglycerol (DPPG), dipalmitoyl phosphatidylethanolamine (DPPE), dipalmitoyl phosphatidylinositol (DPPI), dipalmitoyl phosphatidylserine (DPPS), *N*-palmitoylsphingomyelin, cholesterol, and palmitic acid. This composition was chosen considering the chemical composition of the lung surfactant Survanta® but excluding the surfactant proteins B and C (SP-B and SP-C) due to limitations of the simulation design. The lipid proportions used in the lung surfactant model are described in Table 3. *N*-palmitoylsphingomyelin was chosen to represent the sphingomyelins from the surfactant composition; palmitic acid was chosen as a generic fatty acid, and dipalmitoyl phosphatidyl represented the phospholipid tails since it is the most relevant one in bovine lung surfactant (18). This simplification was done considering that only the polar head interactions would be relevant in the simulation.

1.5. Molecular Dynamics Simulation. All simulations were performed using the Gromacs 2021.1 program and the Gromos54a7 force field. The force field parameters were obtained from the automated topology builder. After the system was built, an energy minimization was performed to relax the system and remove any overlapping atoms due to the system construction. The minimization was set to converge when the system reached $1,000 \text{ kJ mol}^{-1} \text{ nm}^{-1}$, and the steepest descent method was used. Then, a 50-ns simulation using the N_T ensemble (that refers respectively to the number of particles, surface tension and temperature, that are controlled in the simulation) was performed to equilibrate the system temperature at 298 K and surface tension at 20 mN/m. The PS molecule at the center had its position restrained with the force constant of $1,000 \text{ kJ mol/nm}^2$ in every atom and in all directions. The Berendsen pressure coupling was used along with the velocity rescale thermostat. The time constant

was 0.5 ps for the temperature coupling and 2.0 ps for the pressure coupling. The compressibility was set to $4.5 \times 10^{-5} \text{ bar}^{-1}$ in the xy plane and to 0 bar^{-1} in the z axis. Finally, a 200-ns simulation was performed using the same parameters described above. The position restraints were removed, and the PS molecule was set free to move in any direction. The Particle-Mesh Ewald electrostatics algorithm was used with a cutoff for short-range and long-range van der Waals and Coulomb interactions of 1.2 nm and a time step of 2 fs.

The tridimensional diffusion coefficient (D_{xyz}) of the PS molecule in the lung surfactant model is estimated from the slope of the mean square displacement (MSD) vs. the time plot as follows:

$$D_{xyz} = \lim_{t \rightarrow \infty} \frac{1}{2Nt} \frac{d}{dt} \langle \|R_i(t+t_0) - R_i(t)\|^2 \rangle_{t_0}$$

where N is the dimension of the translation (i.e., equal to three), i is the PS molecule, and $R_i(t)$ is the vector of the position for the center of mass (COM) for the PS molecule. The MSD was averaged over time t . The diffusion coefficient was calculated by using least squares fitting of the MSD data from 50 to 150 ns. The radius of gyration (R_g) of each PS was also determined as follows:

$$R_g = \sqrt{\frac{\sum_i m_i \|r_i\|^2}{\sum_i m_i}}$$

where m_i is the mass of atom i and r_i is the position of atom i with respect to the COM of the PS molecule.

2. Results

2.1. PDI of *S. pneumoniae*. All of the tested PSs are effective against *S. pneumoniae*. However, as it is evident in Fig. 1, most of them have their phototoxicity significantly suppressed in the presence of Survanta®. ICG has a moderate PDI effect in the presented concentration that is completely inhibited when the lung surfactant is present. PDZ achieves complete inactivation of the bacteria at a low concentration (100 nm) in PBS, but this effect also completely disappears with 5% Survanta®. For BC-t and PpIX, there is mild bacterial inactivation in the presence of Survanta®, but it is much lower than the complete inactivation achieved in PBS. The only exception to the suppression of the inactivation seems to be MB, for which there is no difference between the PBS and the 5% Survanta groups. The PDI with 1 μM MB has a partial response with a fluence of 10 J/cm^2 but reaches complete inactivation with 20 J/cm^2 . The presence of the lung surfactant has no effect on the photodynamic effect of MB.

2.2. Optical Properties. Changes in absorbance and fluorescence spectra are indicative of changes in the local field of interaction of a molecule, which directly changes the energy required for the electrons to be promoted to excited states. The absorbance spectra for the five PSs in PBS with and without 5% Survanta® in the

Table 3. Lipid composition and proportion used in the monolayer simulations in comparison with the Survanta lipid composition as the reference proportion

| Lipid | No. of molecules | Model composition (% [m/m]) | Survanta lipid composition (% [m/m]) (33) |
|----------------------------------|------------------|-----------------------------|---|
| DPPC | 50 | 55.45 | 50.00 |
| POPC | 21 | 24.11 | 21.00 |
| DPPG | 3 | 3.28 | 2.40 |
| DPPE | 4 | 4.18 | 3.40 |
| DPPI | 1 | 1.23 | ~0.65 |
| DPPS | 1 | 1.11 | ~0.65 |
| <i>N</i> -palmitoylsphingomyelin | 4 | 4.25 | 3.40 |
| Cholesterol | 1 | 0.58 | <0.20 |
| Fatty acids | 15 | 5.81 | 5.80–14.00 |

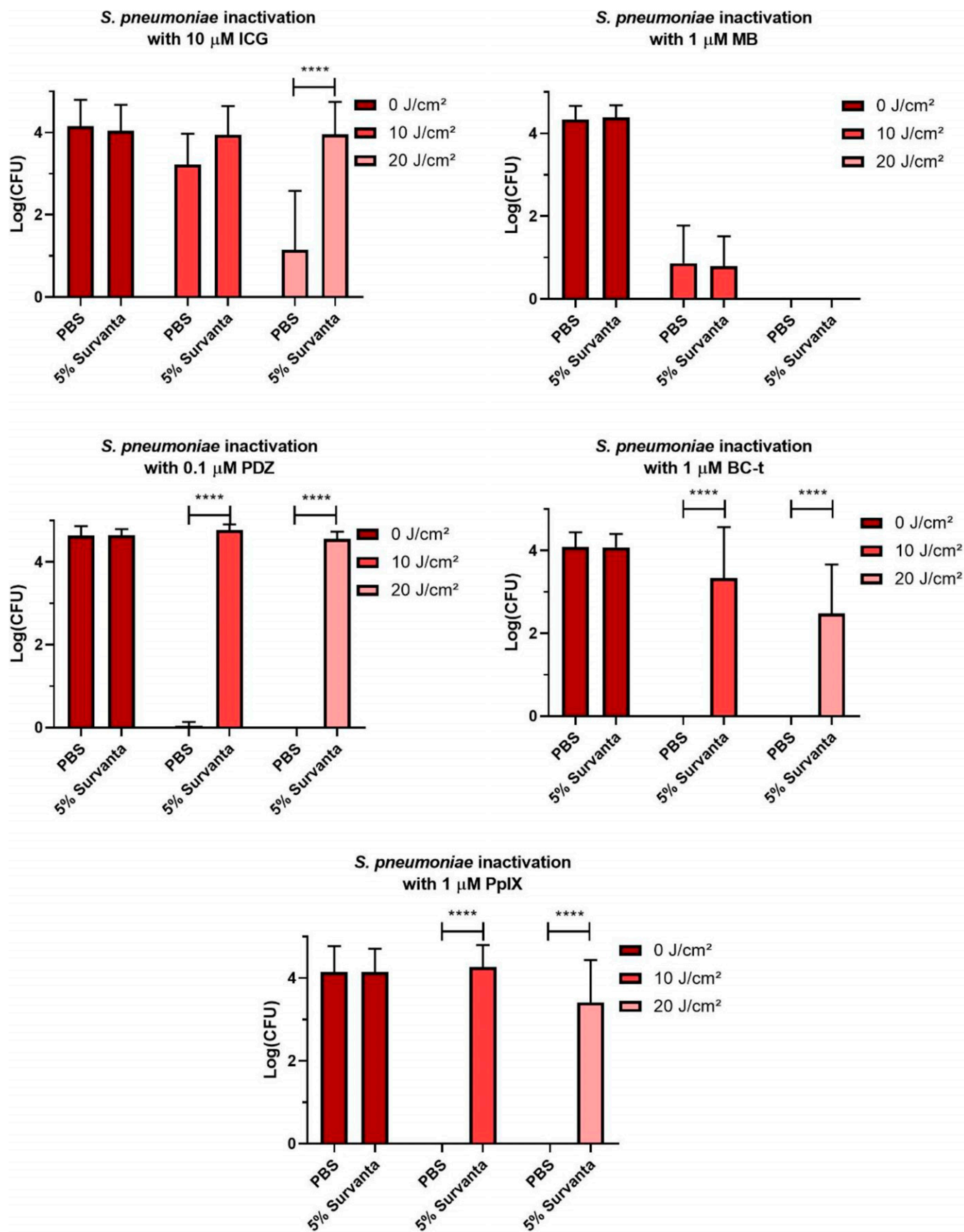


Fig. 1. PDI of *S. pneumoniae* using different PSs and wavelengths (808 nm for ICG, 660 nm for all others) in PBS with or without 5% of the medical-grade lung surfactant Survanta®. CFU: colony-forming units. **** $P < 0.001$.

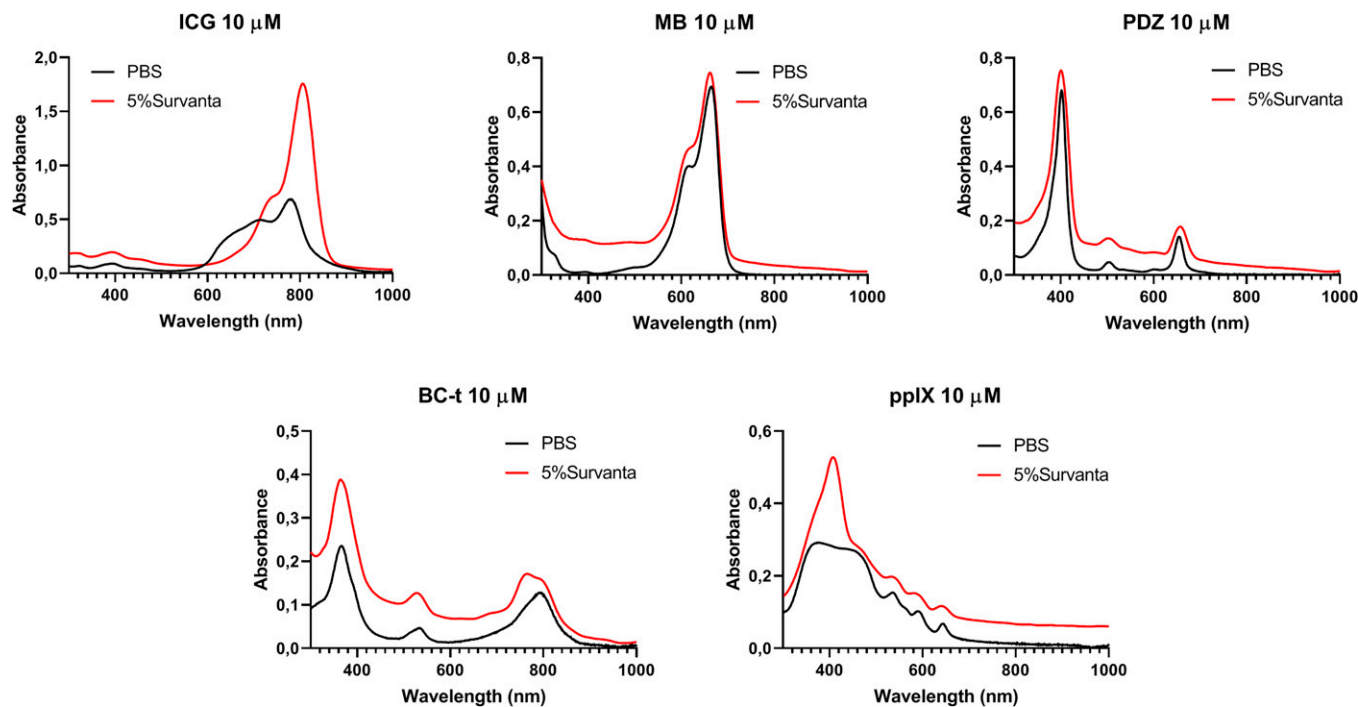


Fig. 2. Absorbance spectra of the five PSs in PBS with and without 5% Surfactant®.

spectral range of 300 to 1,000 nm are presented in Fig. 2. The presence of the lung surfactant consistently increases the absorbance of the PSs, which suggests an interaction between them. For MB and PDZ, no dislocations are observed in the spectra with and without Surfactant®. In the case of BC-t, the characteristic peak at 793 nm is slightly shifted to 762 nm.

For ICG and PpIX, the spectra in PBS are consistent with the formation of aggregates. The addition of 5% Surfactant® shows spectral evidence of a decrease in aggregation and an increase of the higher-absorbing monomer forms. It is known that, in ionized solutions, the tendency to form aggregates is highly probable (26). For ICG in PBS, that is seen in the absorbance in the 600- to 705-nm range, where there is a band associated with H aggregates. In this solvent, the maximum absorbance of the ICG monomer peaks in 780 nm. ICG in 5% Surfactant® shows a red shift of the maximum absorption peak (to 806 nm), and lower absorption in the 600- to 705-nm band suggests a decrease in the concentration of H aggregates. In the case of PpIX, the Soret band peaks at 379 nm in PBS, while in 5% Surfactant®, it shifts to 406 nm and has a drastic increase, which can also be associated with a reduced concentration of aggregates.

The fluorescence emission spectra presented in Fig. 3 were recorded in PBS with and without 5% Surfactant® at room temperature. The emission of the PSs can be affected by the presence of lung surfactant in different ways. For ICG and PpIX, the most affected in terms of absorbance, there is a shift in the emission peak toward higher wavelengths but without significant change in intensity. The fluorescence intensity of MB decreases slightly, and the one of PDZ increases slightly. For BC-t, the fluorescence signal is enhanced dramatically.

Despite the modifications seen in the absorbance and fluorescence spectra, the impact of Surfactant® in the photobleaching rate of the PSs is either small or not significant (Fig. 4). This rate is an indirect measure of the photodynamic effect since the ROS generated will eventually destroy the PS and decrease the sample's absorbance. For ICG and MB, the statistical analysis showed that the normalized absorbance is significantly smaller

after 15 and 20 J/cm² of light treatment when Surfactant® is present, indicating a higher photobleaching rate. For PDZ, BC-t, and PpIX, the addition of 5% Surfactant® does not affect this phenomenon. This suggests that the interaction between the PSs and the lung surfactant does not decrease the probability of encounter with the O₂ nor the formation of reactive species.

2.3. Molecular Dynamics. The simulations have shown that all PSs interacted with the phospholipid polar heads during most of the simulation time. The molecules have an affinity for the phospholipid polar groups (*SI Appendix, Fig. S3*). The *z*-profile analyses (Fig. 5) describe where the *z* component of the molecule's COM is located over the simulation time. By plotting the *z* component of the polar heads' COM, it is possible to note that most of the PS molecules almost immediately migrate to the polar heads region, where they remain for the rest of the simulation. The only exception is MB, which first interacts with the upper monolayer (first dozen of nanoseconds), only to break free and interact with the lower monolayer until roughly 50 ns. After that, the molecule seems to be rather loose in the aqueous phase until right before 100 ns, when it settles in the lower monolayer for the rest of the simulation.

The radial distribution function analysis quantifies the proximity between the PS molecules and the lipids around them during the simulation. The graphs in Fig. 6 show the density distribution of certain lipids along the distance from the molecules. The data are averaged over the last 100 ns. Thus, it is possible to observe whether a PS molecule has any particular affinity for a specific lipid. Most molecules are closer to DPPC and/or POPC molecules (those molecules show peaks around 0.5 nm) since they are the most abundant lipids. Noticeably, positively charged molecules, such as BC-t and MB, interact with both negatively charged and zwitterionic lipids, while negatively charged molecules, such as ICG, PDZ, and PpIX, interact only with zwitterionic lipids.

Table 4 shows the diffusion coefficient and the radius of gyration estimated in the molecular simulation for each PS interacting with polar heads of phospholipids found in the lung

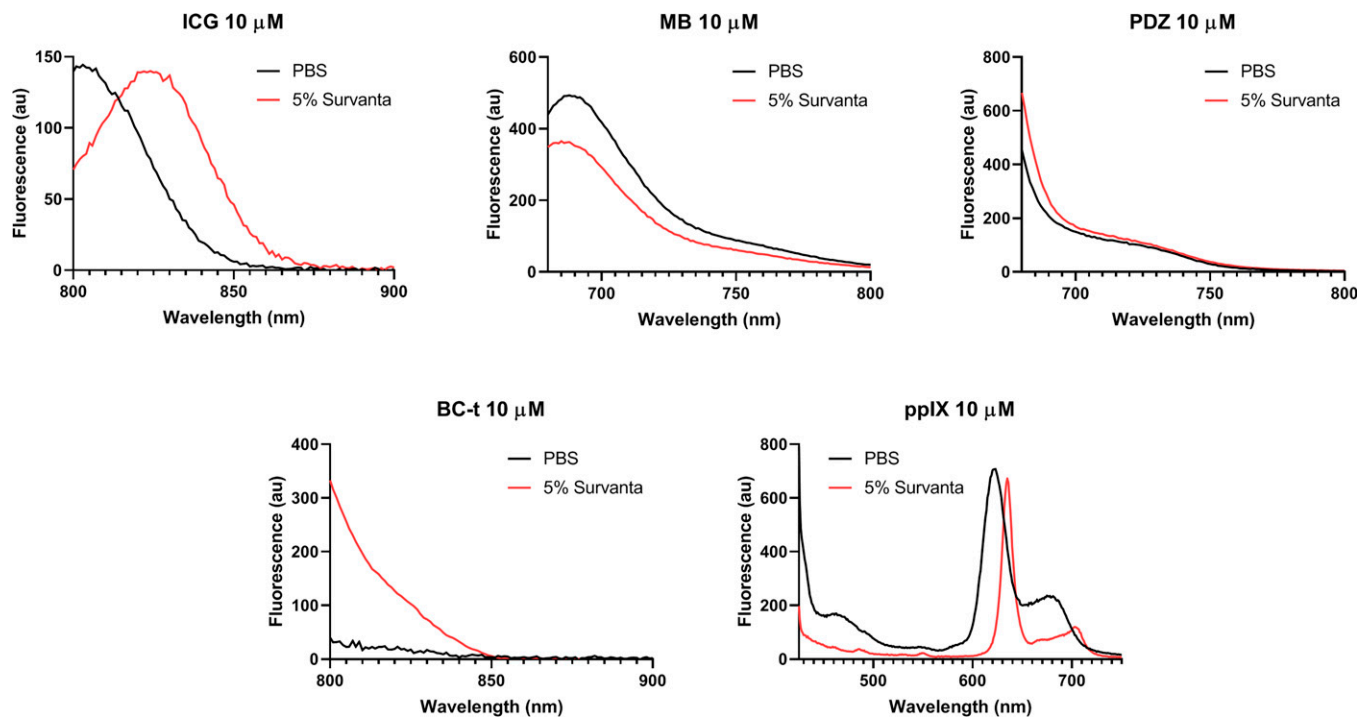


Fig. 3. Fluorescence spectra of the five PSs in PBS with and without 5% Survanta®. Au: arbitrary units.

surfactant model. These properties may infer the mobility of the PS during the molecular simulation after it attaches to polar heads, which is a good indication for inhibition of the microbial activity seen in Fig. 1. MB presents the largest diffusion coefficient and the smallest radius of gyration of the five PSs, which could explain the differences seen in Figs. 1 and 5.

3. Discussion

The interaction with the lung surfactant negatively impacts the efficacy of many pulmonary medications, and the results of this research have shown that this is also the case for multiple PSs.

The molecules selected for this study presented different chemical properties (Table 1), including molar mass, net electric charge, and polarity, as well as different photochemical properties, with varying molecular absorption coefficients and singlet oxygen formation quantum yields. All of them had potential for the PDI of bacteria, as became evident in Fig. 1, since they all significantly reduced the viability of *S. pneumoniae* in PBS. However, because of their chemical and photochemical differences, the concentration of each PS required for this effect varied in over 100-fold. Namely, PDZ completely eliminated the bacteria at 100 nM, while ICG only had a partial response at 10 μM. Yet, in the presence of the lung surfactant Survanta®, the inactivation effect of

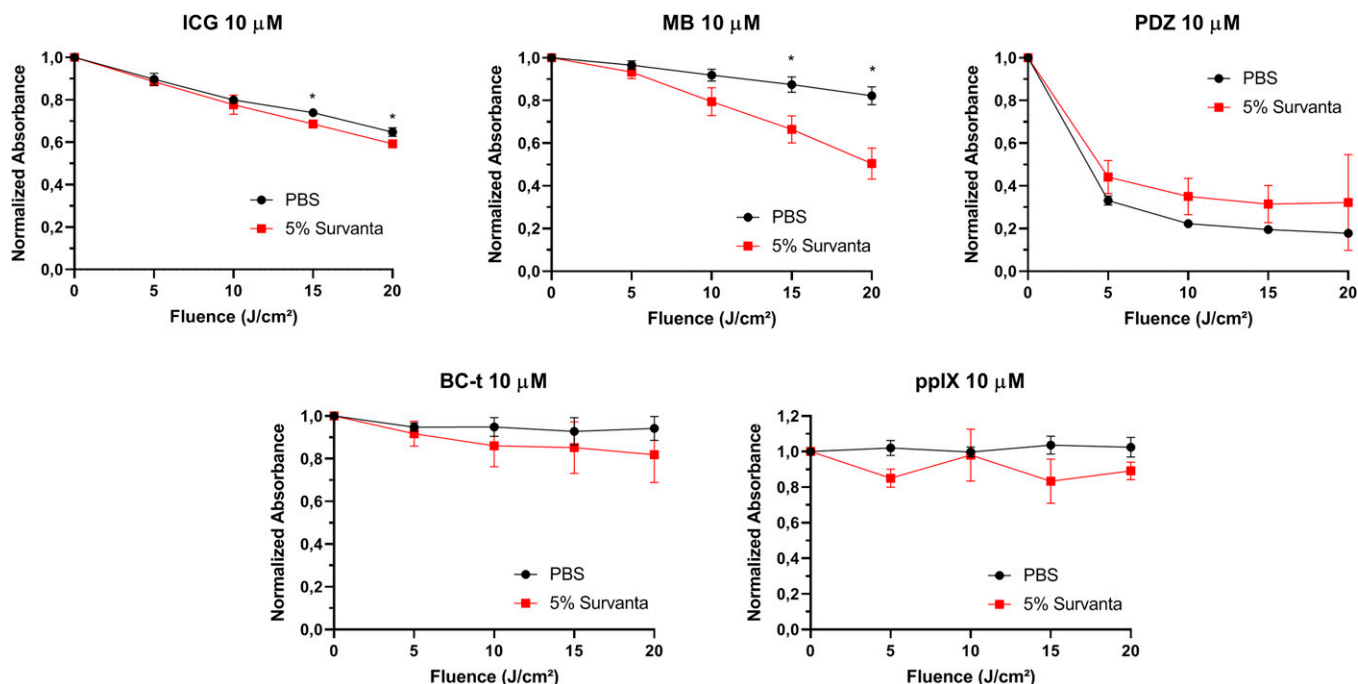


Fig. 4. Photobleaching profile of the five PSs in the presence or absence of 5% Survanta®. * $P < 0.05$.

PDZ was completely suppressed, and it showed no antimicrobial response. The same occurred for the less potent ICG. In the case of PpIX and BC-t, which were both completely effective at 1 μM in PBS, only a partial response was obtained in the presence of 5% Survanta[®]. Despite the different properties of these four PSs, Survanta[®] consistently inhibited the PDI effect for all of them. On the other hand, MB seemed to be an exception to this rule and at 1 μM , showed a partial killing of *S. pneumoniae* with 10 J/cm² and a complete killing with 20 J/cm² in both the presence and absence of the lung surfactant.

The aPDT effect of ICG had been previously reported to be inhibited in the presence of horse plasma, and two mechanisms were proposed to explain it: quenching of the singlet oxygen produced or inhibition of the uptake by the target organisms (27). So, we proposed to test if either of these mechanisms played a role in the inhibition of the PDI by 5% Survanta[®]. The spectral modifications shown in Figs. 2 and 3 suggest a change in the environment surrounding the PS molecules, which indicates that there is a strong chemical interaction between them and the molecules present in the lung surfactant. However, Fig. 4 shows that this interaction does not inhibit the formation of ROS nor quenches their activity. If there was a direct quenching effect, say by the presence of a molecule much more likely to be targeted by them than others, there would be a reduction of the photobleaching of the PS because it would be less likely to be destroyed by the oxidative stress. Instead, what occurs is either an increase or maintenance of the photobleaching rate.

Thus, we propose that the interaction between the PS and the phospholipid components of the lung surfactant could hinder the molecular attachment to the bacterial wall, similarly to what happens to antimicrobial peptides (19). The interaction with the bacterial wall seems to be fundamental for the mechanism of action of antimicrobial PSs (28). The molecular dynamics simulation was used to test if this was the case: in particular, to bring more information regarding the mobility of the PS in the presence of the lung surfactant, which correlates to its availability to interact with the target (in this case, the bacteria). Overall, the simulation shows that all PSs interact with the phospholipid mixture, as made clear by comparing *SI Appendix*, Figs. S2 and S3. Fig. 6 shows that each molecule preferably interacts with specific phospholipids in the surfactant layer. ICG interacts mostly with DPPC, the most abundant component of Survanta[®]. BC-t either also interacts with DPPC or interacts with the second most frequent component, POPC. The chlorin e₆ portion of PDZ mostly interacts with POPC. As for PpIX, the molecule is close to a DPPG-rich region, but there is also proximity to DPPC. MB is closer to DPPG and palmitic acid molecules, which make up a smaller portion of the composition of the surfactant.

Besides the specific interaction with less abundant phospholipids, another result that separates MB from the other PSs is the Z profile, shown in Fig. 5. For ICG, BC-t, PpIX, and the chlorin e₆, there is a strong adherence to the surfactant layer that occurs in the first few nanoseconds, and they do not release from this

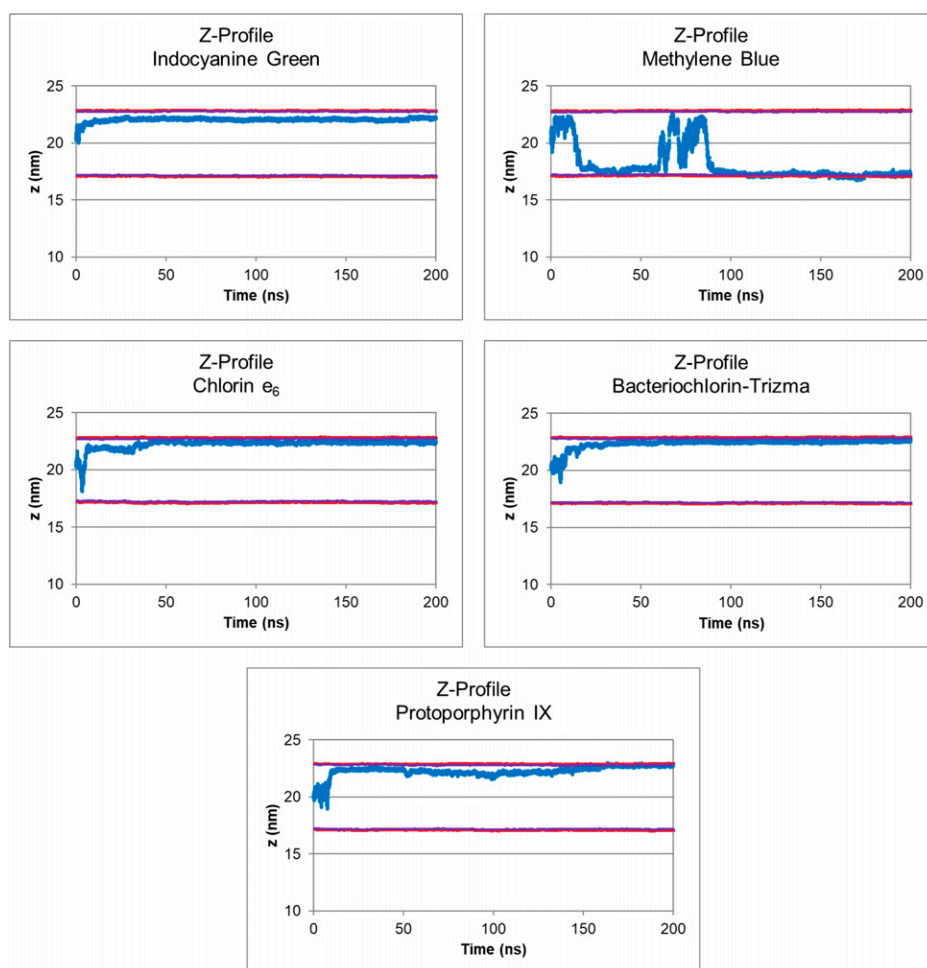


Fig. 5. Z-profile graphs for each PS molecule. The red points mark the z component of phosphate groups' COM, whereas the purple points mark the z component of choline groups' COM. The blue points mark the z component of the PS molecule's COM.

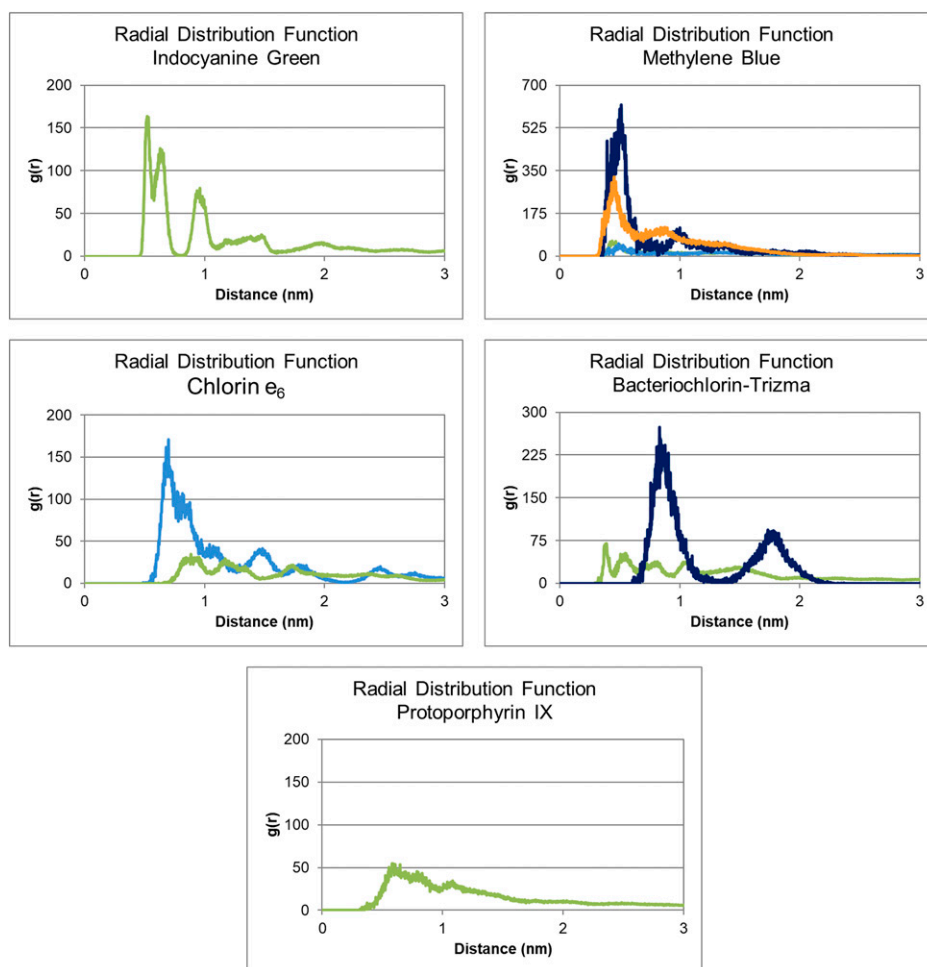


Fig. 6. Radial distribution function graphs of the last 100 ns of all simulations. The reference groups are the closest atoms to the monolayer charged groups. Green, DPPC phosphate groups; light blue, POPC phosphate groups; darker blue, DPPG phosphate groups; orange, palmitic acid polar groups. Other lipids/components were omitted from the visualization in each graph due to not having peaks below 1 nm.

layer during the entire simulation (200 ns). On the other hand, MB interacts and is released from the surfactant multiple times over the course of the simulation, and it even interacts with both the upper and lower layers. MB is the most water soluble of the five PSs (as seen on $\log P$ values in Table 1), which is a likely explanation for this behavior. Moreover, MB has one positive charge distributed along the molecule, which might result in a strong interaction with the DPPG (or other negatively charged phospholipids, such as DPPE or DPPI) polar heads. This could explain the MB molecule's accommodation in the polar heads after 100 ns since DPPG molecules are negatively charged. The other molecules, despite having positive or negative net charges, have more than one charged group, which might also result in a strong interaction with both positive and negative charges present in the polar heads. Thus, despite our Survanta® lung surfactant model having a negative net charge, free energy analyses might be necessary to evaluate the strength of the interaction with the polar heads. The estimated diffusion coefficient and radius of gyration (Table 4) are probably more significant for the overall effect. The radius of gyration of each PS molecule is similar in magnitude to the hydrodynamic radius. The mobility of nonspherical particles may be described by the hydrodynamic radius that is related to the frictional force of particle with the solvent. MB molecules present the smallest radius of gyration compared with the other PSs, meaning that MB has the largest mobility.

Thus, there seems to be a correlation between the loss of mobility of a PS in the presence of Survanta® and its loss in

efficacy against bacteria. As expected, the lung surfactant is a barrier to be transposed for the success of the photodynamic treatment of pneumonia. Still, different approaches can be taken to make this possible. On one hand, MB might seem to be the obvious choice for future studies since it retained its PDI efficacy despite the presence of Survanta®. However, some of MB's photochemical characteristics are not ideal for this application. Because of the pathology and infectious nature of pneumonia, the best treatment for it needs to be as little invasive as possible, and in the case of aPDT, that relies on using an external light source, with a wavelength able to penetrate through multiple layers of biological tissue. We have gathered enough evidence to believe that would be possible using 808 nm and ICG, but it would not be able to activate MB with this wavelength (13, 29).

Table 4. Estimated diffusion coefficient (D_{xyz}) in centimeters squared per second and radius of gyration (R_g) in nanometers for each PS in the molecular simulation with their 10-fold SDs (10σ)

| PS | D_{xyz} (10^{-8} cm ² /s) | R_g (nm) |
|------|---|-------------|
| ICG | 141 ± 8 | 0.66 ± 0.05 |
| MB | 259 ± 2 | 0.38 ± 0.03 |
| PDZ | 144 ± 3 | 0.47 ± 0.06 |
| BC-t | 164 ± 3 | 0.51 ± 0.10 |
| PpIX | 216 ± 6 | 0.50 ± 0.10 |

On the other hand, it might be possible to still use the PSs that strongly interact with the lung surfactant. In studies where a similar problem was identified for other drugs, formulations were proposed as a solution: using the lung surfactant itself as a vehicle (21, 30); encapsulating the active principles into nanoparticles or optimizing nanoparticle design (16, 17, 24, 25, 31, 32); or even using perfluorocarbons, which are pulmonary liquid ventilation agents (33, 34). Also, it is important to consider that the reduced mobility will decrease the local concentration of PS available to interact with the target, but it will not be zero. The bactericidal effect of aPDT of a given context depends on a relationship between the PS concentration and the light dose, in which the larger one of them is, the smaller the other one is required to be [a complete description of the mathematical model is in Willis et al. (35)]. In other words, if there is a lower availability of PS, an increase in light dose might be enough to yield the same effect. An increase in the delivered dose of PS will also increase its locally available concentration, facilitating the killing of bacteria. However, there would be a need to consider the safety of the pulmonary epithelium in this case as well as the integrity of the lung surfactant itself, which is essential for the survival of the patient.

4. Conclusion

aPDT has the potential to be a successful treatment for multiple infectious agents of pneumonia. However, this study shows that the interaction of the lung surfactant with the PS must be considered when developing pulmonary aPDT protocols. The presence of the clinical surfactant Survanta® decreases the

PDI effect of ICG, PDZ®, Bc-t, and PpIX against *S. pneumoniae*. MB is the only PS tested that did not lose efficacy when the lung surfactant was added. This is likely due to a higher mobility of this molecule when interacting with the lung surfactant, consequence of its high water solubility and positive charge. However, since other properties may deem other PSs more appropriate for the treatment of pneumonia, there are formulation strategies that can be used to overcome the lung surfactant interaction. Nonetheless, with all the accumulated evidence that pulmonary aPDT could work, overcoming the lung surfactant barrier might be the main obstacle to its success.

Data Availability. All study data are included in the article and/or *SI Appendix*.

ACKNOWLEDGMENTS. We thank Professors Kleber T. de Oliveira and Clóvis W. O. de Souza from the Federal University of São Carlos for providing the Bc-t. We acknowledge support from São Paulo Research Foundation Grants 2013/07276-1, 2014/50857-8, 2014/50983-3, and 2018/18188-0; National Council for Scientific and Technological Development Grants 465360/2014-9, 465259/2014-6, 305795/2016-3, and 302554/2017-3; Coordination for the Improvement of Higher Education Academic Excellency Program (CAPES PROEX) Grant 88887.602983/2021-00 (Finance Code 001); Rio de Janeiro Research Foundation (FAPERJ) NanoSaúde Research Network Grant E-26/010.000983/2019; FAPERJ Grant 210.104/2020; Brazilian Company of Research and Industrial Innovation (EMBRAPPI) and MM Optics Project PIFS-2005.0022.

Author affiliations: ^aSão Carlos Institute of Physics, University of São Paulo, São Carlos, São Paulo 13566-590, Brazil; ^bDepartment of Chemistry, Pontifical Catholic University of Rio de Janeiro, Rio de Janeiro 22453-900, Brazil; and ^cHagler Institute for Advanced Studies, Texas A&M University, College Station, TX 77843

1. C. Troeger et al.; GBD 2016 Lower Respiratory Infections Collaborators, Estimates of the global, regional, and national morbidity, mortality, and aetiologies of lower respiratory infections in 195 countries, 1990-2016: A systematic analysis for the Global Burden of Disease Study 2016. *Lancet Infect. Dis.* **18**, 1191-1210 (2018).
2. B. T. Bradley, A. Bryan, Emerging respiratory infections: The infectious disease pathology of SARS, MERS, pandemic influenza, and Legionella. *Semin. Diagn. Pathol.* **36**, 152-159 (2019).
3. T. Maisch, Anti-microbial photodynamic therapy: Useful in the future? *Lasers Med. Sci.* **22**, 83-91 (2007).
4. N. Kashef, M. R. Hamblin, Can microbial cells develop resistance to oxidative stress in antimicrobial photodynamic inactivation? *Drug Resist. Updat.* **31**, 31-42 (2017).
5. M. Wainwright et al., Photoantimicrobials-are we afraid of the light? *Lancet Infect. Dis.* **17**, e49-e55 (2017).
6. T. Dai, Y. Y. Huang, M. R. Hamblin, Photodynamic therapy for localized infections: State of the art. *Photodiagn. Photodyn. Ther.* **6**, 170-188 (2009).
7. M. C. Geralde et al., "Pulmonary decontamination for photodynamic inactivation with extracorporeal illumination" in *Proceedings of the SPIE, Endoscopic Microscopy IX and Optical Techniques in Pulmonary Medicine* (SPIE BIOS, San Francisco, CA, 2014), vol. **8927**, p. 89271B-6.
8. I. S. Leite et al., "Photodynamic inactivation of microorganisms which cause pulmonary diseases with infrared light: An in vitro study" in *Proceedings of the SPIE, Endoscopic Microscopy IX and Optical Techniques in Pulmonary Medicine* (SPIE BIOS, San Francisco, CA, 2014), vol. **8927**, p. 89271A-7.
9. I. S. Leite et al., Near-infrared photodynamic inactivation of *S. pneumoniae* and its interaction with RAW 264.7 macrophages. *J. Biophotonics*, **10**, 1002/|bio.201600283 (2018).
10. G. Kassab et al., Nebulization as a tool for photosensitizer delivery to the respiratory tract. *J. Biophotonics* **12**, e201800189 (2019).
11. T. W. Wong et al., Indocyanine green-mediated photodynamic therapy reduces methicillin-resistant *Staphylococcus aureus* drug resistance. *J. Clin. Med.* **8**, 411 (2019).
12. G. Kassab et al., Safety and delivery efficiency of a photodynamic treatment of the lungs using indocyanine green and extracorporeal near infrared illumination. *J. Biophotonics* **13**, e202000176 (2020).
13. J. S. D. Tovar, G. Kassab, H. H. Buzzá, V. S. Bagnato, C. Kurachi, Photodynamic inactivation of *S. pneumoniae* with external illumination at 808 nm through the ex vivo porcine thoracic cage. *J. Biophotonics* **15**, e202100189 (2021).
14. C. M. Cassidy et al., Drug and light delivery strategies for photodynamic antimicrobial chemotherapy (PACT) of pulmonary pathogens: A pilot study. *Photodiagn. Photodyn. Ther.* **8**, 1-6 (2011).
15. J. Lehmann et al., Improvement of pulmonary photodynamic therapy: Nebulisation of curcumin-loaded tetraether liposomes. *Pharmaceutics* **13**, 1243 (2021).
16. E. Baghdan et al., Development of inhalable curcumin loaded nano-in-microparticles for bronchoscopic photodynamic therapy. *Eur. J. Pharm. Sci.* **132**, 63-71 (2019).
17. C. Garcia-Mouton, A. Hidalgo, A. Cruz, J. Pérez-Gil, The lord of the lungs: The essential role of pulmonary surfactant upon inhalation of nanoparticles. *Eur. J. Pharm. Biopharm.* **144**, 230-243 (2019).
18. P. L. Oseliero Filho et al., Structure and thermotropic behavior of bovine- and porcine-derived exogenous lung surfactants. *Langmuir* **36**, 14514-14529 (2020).
19. L. M. P. Souza, J. B. Nascimento, A. L. Romeu, E. D. Estrada-López, A. S. Pimentel, Penetration of antimicrobial peptides in a lung surfactant model. *Colloids Surf. B Biointerfaces* **167**, 345-353 (2018).
20. S. Ortiz-Collazos et al., Interaction of levofloxacin with lung surfactant at the air-water interface. *Colloids Surf. B Biointerfaces* **158**, 689-696 (2017).
21. B. J. H. Banaschewski et al., Antimicrobial and biophysical properties of surfactant supplemented with an antimicrobial peptide for treatment of bacterial pneumonia. *Antimicrob. Agents Chemother.* **59**, 3075-3083 (2015).
22. J. A. Silverman, L. I. Mortin, A. D. G. Vanpraagh, T. Li, J. Alder, Inhibition of daptomycin by pulmonary surfactant: In vitro modeling and clinical impact. *J. Infect. Dis.* **191**, 2149-2152 (2005).
23. E. D. Estrada-López, E. Murce, M. P. P. Franca, A. S. Pimentel, Prednisolone adsorption on lung surfactant models: Insights on the formation of nanoaggregates, monolayer collapse and prednisolone spreading. *RSC Advances* **7**, 5272-5281 (2017).
24. F. R. Souza, L. M. P. Souza, A. S. Pimentel, Permeation of beta-defensin-3 encapsulated with polyethylene glycol in lung surfactant models at air-water interface. *Colloids Surf. B Biointerfaces* **182**, 110357 (2019).
25. F. R. Souza et al., Polymer-coated gold nanoparticles and polymeric nanoparticles as nanocarrier of the BP100 antimicrobial peptide through a lung surfactant model. *J. Mol. Liq.* **314**, 113661 (2020).
26. J. S. Diaz Tovar, G. Kassab, N. M. Inada, V. Salvador Bagnato, C. Kurachi, "Photodegradation in the infrared region of indocyanine green in aqueous solution" in *2019 SBPhoton International Optics and Photonics Conference, SBPhoton IOPC 2019* (IEEE, Sao Paulo, Brazil, 2019), pp. 1-5.
27. G. S. Omar, M. Wilson, S. P. Nair, Lethal photosensitization of wound-associated microbes using indocyanine green and near-infrared light. *BMC Microbiol.* **8**, 111 (2008).
28. S. George, M. R. Hamblin, A. Kishen, Uptake pathways of anionic and cationic photosensitizers into bacteria. *Photochem. Photobiol. Sci.* **8**, 788-795 (2009).
29. G. Kassab, J. S. D. Tovar, H. H. Buzzá, C. Kurachi, V. S. Bagnato, "Non-invasive activation of photosensitizers in the lungs: Achievable goal or impossible dream?" in *Book of Abstracts of the 19th Congress of the European Society for Photobiology*, p. 114 (Eigenverlag, 2021). ISBN 978-3-200-07802-4.
30. A. Van Veen, J. W. Mouton, D. Gommers, B. Lachmann, Pulmonary surfactant as vehicle for intratracheally instilled tobramycin in mice infected with *Klebsiella pneumoniae*. *Br. J. Pharmacol.* **119**, 1145-1148 (1996).
31. O. Cañadas, A. García-García, M. A. Prieto, J. Pérez-Gil, Polyhydroxyalkanoate nanoparticles for pulmonary drug delivery: Interaction with lung surfactant. *Nanomaterials (Basel)* **11**, 1482 (2021).
32. F. Mousseau, J. F. Berret, The role of surface charge in the interaction of nanoparticles with model pulmonary surfactants. *Soft Matter* **14**, 5764-5774 (2018).
33. M. P. Krafft, "Perfluorocarbons and perfluorocarbon emulsions for pulmonary indications" in *The Curious World of Fluorinated Molecules*, K. Seppelt, Ed. (Elsevier, 2021), pp. 219-239.
34. H. J. Lehmler, Perfluorocarbon compounds as vehicles for pulmonary drug delivery. *Expert Opin. Drug Deliv.* **4**, 247-262 (2007).
35. J. A. Willis et al., Photodynamic viral inactivation: Recent advances and potential applications. *Appl. Phys. Rev.* **8**, 021315 (2021).